MBoC | ARTICLE

Cortical tension promotes Kibra degradation via Par-1

Sherzod A. Tokamov[a,b], Stephan Buiter[a], Anne Ullyot[a], Gordana Scepanovic[c], Audrey Miller Williams[a], Rodrigo Fernandez-Gonzalez[d], Sally Horne-Badovinac[a,b], and Richard G. Fehon[a,b,*]

[a]Department of Molecular Genetics and Cell Biology, and [b]Committee on Development, Regeneration, and Stem Cell Biology, The University of Chicago, Chicago, IL 60637; [c]Department of Cell and Systems Biology, and [d]Institute of Biomedical Engineering and Department of Cell and Systems Biology, University of Toronto, Toronto, ON M5G 1M1, Canada

ABSTRACT **The Hippo pathway is an evolutionarily conserved regulator of tissue growth. Multiple Hippo signaling components are regulated via proteolytic degradation. However, how these degradation mechanisms are themselves modulated remains unexplored. Kibra is a key upstream pathway activator that promotes its own ubiquitin-mediated degradation upon assembling a Hippo signaling complex. Here, we demonstrate that Hippo complex-dependent Kibra degradation is modulated by cortical tension. Using classical genetic, osmotic, and pharmacological manipulations of myosin activity and cortical tension, we show that increasing cortical tension leads to Kibra degradation, whereas decreasing cortical tension increases Kibra abundance. Our study also implicates Par-1 in regulating Kib abundance downstream of cortical tension. We demonstrate that Par-1 promotes ubiquitin-mediated Kib degradation in a Hippo complex-dependent manner and is required for tension-induced Kib degradation. Collectively, our results reveal a previously unknown molecular mechanism by which cortical tension affects Hippo signaling and provide novel insights into the role of mechanical forces in growth control.**

Monitoring Editor
Alpha Yap
University of Queensland

Received: Jun 26, 2023
Revised: Oct 17, 2023
Accepted: Oct 20, 2023

SIGNIFICANCE STATEMENT

- The mechanisms by which mechanical tension controls Hippo pathway signaling remain poorly understood. This study focuses on the effects of tension on abundance of a key pathway component, Kibra.
- Using a combination of genetic and acute experimental manipulations, the authors show that increased cortical tension promotes Kibra degradation.
- Further, the kinase Par-1, which is strongly recruited to the cell cortex under conditions of high cortical tension, is necessary for this effect. These findings suggest that mechanical tension regulates tissue growth in part by promoting Kibra degradation, thereby inhibiting Hippo pathway signaling.

This article was published online ahead of print in MBoC in Press (http://www.molbiolcell.org/cgi/doi/10.1091/mbc.E23-06-0246) on October 30, 2023.

*Address correspondence to: Richard G. Fehon (rfehon@uchicago.edu).

Abbreviations used: Kib, Kibra; MRLC, myosin regulatory light chain; RhoGEF2, Rho guanine exchange factor 2; SCF, Skp1-Cul1-F-box-protein; Yki, Yorkie.

INTRODUCTION

Elucidating the mechanisms that ensure robustness and reproducibility of organ size is a fundamental problem in cell and developmental biology. A key regulator of tissue growth in animals is the Hippo pathway. At its core, the Hippo pathway consists of a kinase cascade, composed of Ser/Thr kinases Hippo (Hpo) and Warts (Wts) and scaffold proteins Salvador (Sav) and Mats that inhibits nuclear translocation of a pro-growth transcriptional coactivator, Yorkie (Yki). The activity of the kinase cascade is regulated by multiple upstream components, including a multivalent scaffold protein, Kibra (Kib).

Kib localizes at the apical cell cortex of epithelial cells, where together with its binding partner, Merlin (Mer), it plays a key role in assembling and activating the Hippo kinase cascade to repress Yki activity. In the absence of a conventional receptor/ligand pair, however, little is known about how Kib activity is regulated.

A conserved feature of the Hippo pathway is its regulation via forces generated by F-actin and nonmuscle myosin II (actomyosin). Actomyosin forces are regulated by the small GTPase RhoA (Rho1 in Drosophila), which can be activated or deactivated by guanine exchange factors (GEF) or GTPase activating proteins, respectively (Piekny *et al.*, 2005). Rho1 potently stimulates actomyosin contractility by simultaneously activating Diaphanous, a formin that promotes linear F-actin bundle assembly, and Rho kinase (Rok), which phosphorylates and activates the myosin regulatory light chain (Lecuit *et al.*, 2011). Studies over the years have shown that both F-actin polymerization and myosin activation stimulate the activity of Yki and its mammalian homologues, YAP/TAZ (Dupont *et al.*, 2011; Fernandez *et al.*, 2011; Sansores-Garcia *et al.*, 2011; Wada *et al.*, 2011; Aragona *et al.*, 2013; Rauskolb *et al.*, 2014; Ibar *et al.*, 2018). Mechanistically, cytoskeletal tension was shown to promote Yki/YAP activity via LIM domain Ajuba (Jub) family proteins, such as Ajuba, which accumulate at cell–cell junctions in response to tension and sequester Wts (Rauskolb *et al.*, 2014; Pan *et al.*, 2016; Ibar *et al.*, 2018). However, this mechanism acts directly on the core kinase cascade and it remains unclear whether or how tension could regulate the upstream Hippo signaling components, such as Kib.

A key determinant of signaling output downstream of Kib is its protein level. Loss of Kib results in tissue overgrowth via Yki activation, while the opposite occurs under ectopic Kib expression (Baumgartner *et al.*, 2010; Genevet *et al.*, 2010; Yu *et al.*, 2010; Su *et al.*, 2017; Tokamov *et al.*, 2021). Furthermore, upstream regulators, including Mer, Expanded and Kib, are transcriptionally upregulated by Yki, making their abundance a key component of a conserved negative feedback loop (Hamaratoglu *et al.*, 2006; Genevet *et al.*, 2010; Yee *et al.*, 2019). Thus, control of Kib abundance provides an important point for modulating Kib-mediated Hippo pathway activation. In addition to transcriptional regulation, Kib abundance is regulated via ubiquitin-mediated proteolytic turnover (Tokamov *et al.*, 2021). Upon assembly of the Hippo complex, Kib is ubiquitinated via the SCF^{Slimb} E3 ubiquitin ligase and subsequently degraded. This mechanism simultaneously requires a consensus recognition motif in Kib that recruits SCF^{Slimb}, as well as the two N-terminal WW domains in Kib that mediate Hippo complex formation. Notably, Kib levels are elevated in cells with lower cortical tension, suggesting that actomyosin-generated forces could regulate Kib abundance (Tokamov *et al.*, 2021). How Kib levels are modulated by mechanical forces and whether this mechanism involves additional mechanosensitive components remains unknown.

In this study, using genetic, osmotic, and pharmacological manipulations of myosin activity, we report that actomyosin-generated cortical tension modulates Kib abundance. We find that increasing myosin activity and cortical tension lowers Kib abundance, while acutely inhibiting myosin activity elevates Kib levels. Importantly, we find that tension-mediated Kib degradation occurs independently of the previously identified Jub-Wts mechanism. Instead, our results suggest that the serine/threonine kinase Par-1 promotes Kib degradation in a tension dependent manner. Together, our findings provide evidence that tension regulates upstream Hippo signaling and advance our understanding of how mechanical forces can influence the activity of a signaling pathway.

RESULTS

Cortical tension promotes Kib degradation

Previously, we showed that Kib's role in assembling the Hippo signaling complex promotes its own degradation, thereby forming a posttranslational negative feedback loop (Tokamov *et al.*, 2021). Additionally, our results suggested that this feedback mechanism is modulated by cortical tension because cell clones under compression display higher levels of Kib than their neighbors. To better understand how Kib abundance is regulated, we sought to genetically manipulate nonmuscle myosin II (myosin) contractility as a means to affect cortical tension. To visualize Kib, we used Kib tagged with the green fluorescent protein (GFP) and expressed under the ubiquitin promoter (Ubi>Kib–GFP), a transgene that we previously showed to be an effective reporter of posttranslational changes in Kib abundance (Tokamov *et al.*, 2021). We first transiently ectopically expressed RhoGEF2 to activate Rho1 upstream of myosin in the posterior compartment of the wing imaginal disc using the *hh>Gal4* driver combined with ubiquitously expressed $Gal80^{ts}$ (*tub>*$Gal80^{ts}$). Strikingly, expression of RhoGEF2 for 24 h resulted in a significant decrease in Kib levels (Figure 1, A and -B). Using phosphospecific antibody against the phosphorylated myosin regulatory light chain (pMRLC; Zhang and Ward, 2011), we confirmed that myosin activity was upregulated under these conditions (Supplemental Figure S1, A–A″). Additionally, consistent with the function of Kib in repressing Yki and the role of tension in promoting Yki transcriptional activity (Baumgartner *et al.*, 2010; Genevet *et al.*, 2010; Yu *et al.*, 2010; Rauskolb *et al.*, 2014), we saw increased nuclear Yki accumulation upon RhoGEF2 expression (Supplemental Figure S1, B and C). In contrast, the abundance of Ubi>$Kib^{\Delta WW1}$-GFP, a variant of Kib that is insensitive to Hippo complex-mediated degradation (Tokamov *et al.*, 2021), was not affected by RhoGEF2 expression (Figure 1, C and D). These results are consistent with our previous observation that the abundance of wild-type Kib, but not $Kib^{\Delta WW1}$, was elevated in mosaic clones with decreased cortical tension (Tokamov *et al.*, 2021) and suggest that cortical tension regulates Kib abundance via complex-mediated degradation.

We also previously showed that cortically localized Yki promotes myosin activation via a myosin light chain kinase called Stretchin (Strn-MLCK; Xu *et al.*, 2018). Specifically, ectopic expression of myristoylated Yki (myr-Yki) leads to an increase in myosin activation. Because *hh>Gal4* drives expression both in the disk proper and the overlaying peripodial epithelium of the wing imaginal disc, ectopic myr-Yki expression with *hh>Gal4* leads to significant tissue disfigurement (unpublished data), which complicates tissue imaging and analysis. Therefore, we used a different driver, *apterous>Gal4 (ap>Gal4)*, which was previously used to drive myr–Yki expression in the dorsal compartment of the wing primordium and led to significant myosin activation (Xu *et al.*, 2018). As with RhoGEF2, ectopic myr–Yki expression substantially diminished Kib levels (Figure 1, E and F). Depletion of Strn–MLCK strongly suppressed the effect of myr–Yki, suggesting that this effect was mediated via myosin activity (Figure 1, E′ and F). However, Strn–MLCK depletion alone did not increase Kib levels (Figure 1, E″ and F), so the physiological significance of this effect is unclear.

Changes in osmotic conditions alter myosin activity and cortical tension

Our genetic manipulations of cortical tension support the model that tension promotes Kib turnover. We sought to further test this model by acutely manipulating myosin activity and cortical tension. Changes in osmotic pressure have been used extensively to alter

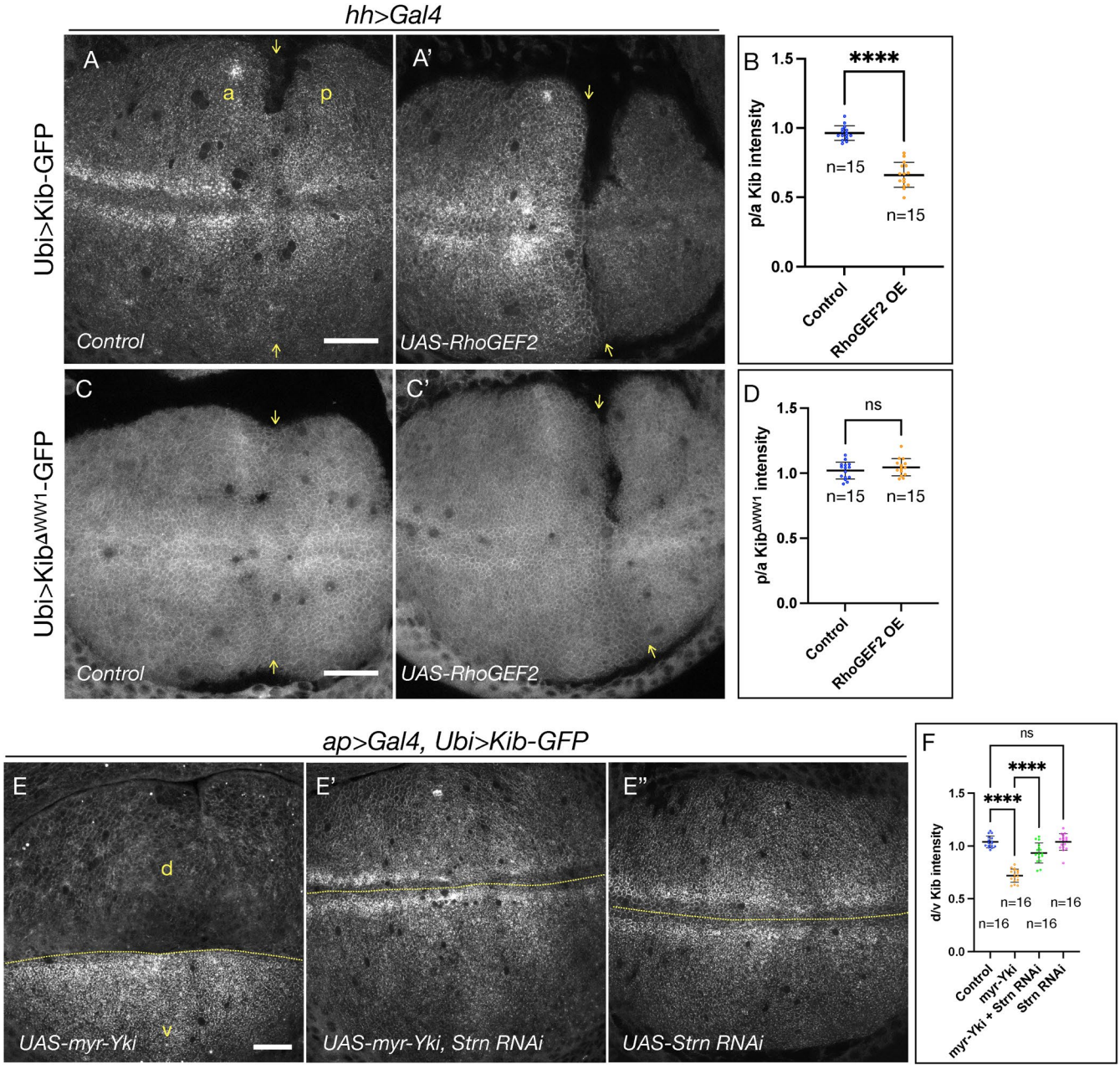

FIGURE 1: Cortical tension promotes Kib degradation. (A and A′) Compared to control tissues (A), ectopic RhoGEF2 expression for 24 hr results in a significant decrease in Kib abundance (A′). Yellow arrows indicate anterior-posterior (a-p) boundary. (B) Plot of p/a ratio of Ubi>Kib-GFP mean fluorescence intensity under the conditions shown in A and A′. (C and C′) In contrast to wild-type Kib, Kib$^{\Delta WW1}$ is not affected by RhoGEF2 expression. (D) Plot of p/a ratio of Ubi>Kib $^{\Delta WW1}$-GFP mean fluorescence intensity under the conditions shown in C and C′. (E–E″) Ectopic myr-Yki expression leads to a significant decrease in Kib abundance (E), and depletion of Strn-MLCK suppresses the effect of myr-Yki expression (E′). Depletion of Strn-MLCK alone has no effect on Kib abundance (E″). Dashed lines indicate the dorsal-ventral (d-v) boundary. Scale bars = 20 μm. (F) Plot of d/v ratio of Ubi>Kib-GFP mean fluorescence intensity under the conditions shown in E–E″ (a representative control image of Ubi>Kib-GFP is shown in A). All experiments were replicated at least three times. Unless indicated otherwise, statistical significance for two group comparisons was calculated using Mann–Whitney test. For more than two groups, One-way ANOVA followed by Tukey's Honestly Significant Difference test was used. Also, unless otherwise noted, n = number of wing disks and data are shown as the mean ± SD and significance values are represented as follows: ****$p \leq 0.0001$, ***$p \leq 0.001$, **$p \leq 0.01$, *$p \leq 0.05$, ns = not significant.

cortical cytoskeletal organization and tension (Di Ciano *et al.*, 2002; Guilak *et al.*, 2002; Boulant *et al.*, 2011; Sinha *et al.*, 2011; Stewart *et al.*, 2011; Pietuch *et al.*, 2013; Diz-Muñoz *et al.*, 2016; Roffay *et al.*, 2021). Recently, we found that relatively mild changes in osmotic conditions can induce dramatic changes in myosin organization in wing imaginal epithelial cells, whereby myosin becomes more junctional under hypotonic and less junctional under hypertonic conditions (Tokamov *et al.*, 2023). Therefore, we sought to test whether these osmotic manipulations also affect myosin activity and cortical tension.

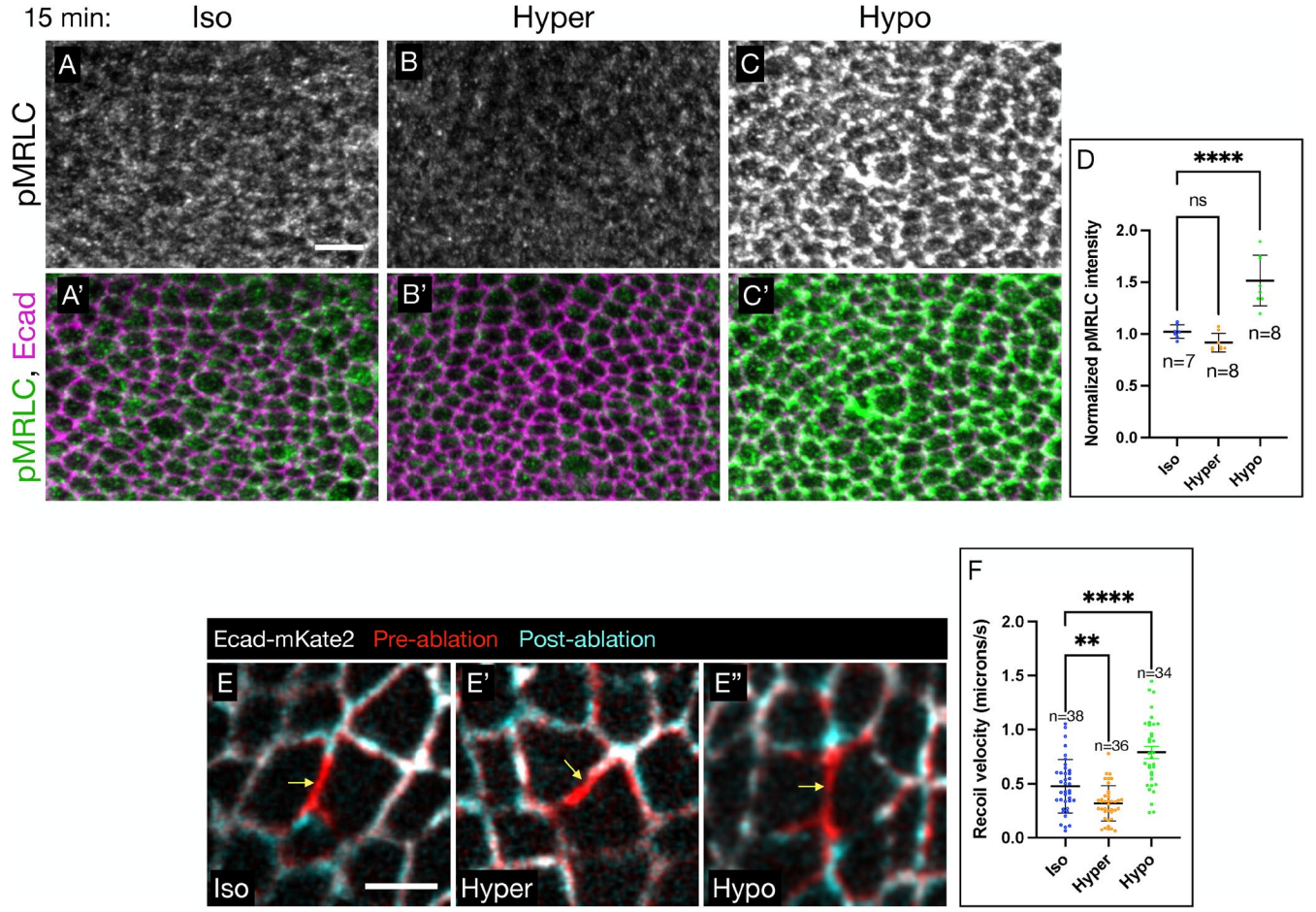

FIGURE 2: Changes in osmotic conditions alter myosin activity and cortical tension. (A–C) Compared to isotonic conditions (A and A'), hypertonic conditions lead to a slight decrease in pMRLC (B and B'), whereas hypotonic conditions significantly increase pMRLC signal (C and C'). Scale bar = 5 μm. (D) Quantification of mean pMRLC intensity under osmotic conditions shown in A–C. (E–E") Representative overlay images of Ecad-mKate2 in wing imaginal disc cells pre- (red) and postablation of bicellular junctions (arrows) under isotonic (E), hypertonic (E'), hypotonic E") conditions. Scale bar = 3 μm. (F) Quantification of initial junction recoil velocities measured from the ablation experiments; *n* = number of ablated junctions (see also Supplemental Figure S2).

We first examined the effect of different osmotic conditions on myosin activity using the anti-pMRLC antibody. Compared to isotonic controls, we saw a slight decrease in pMRLC staining under hypertonic conditions, although this effect was not statistically significant, likely due to high background staining associated with this antibody (Figure 2, A–B' and D). Under hypotonic conditions, however, we observed a substantial increase in pMRLC (Figure 2, C and D), indicating that osmotic manipulations can acutely alter myosin activation. Importantly, overall myosin abundance was not affected by the osmotic shifts (Supplemental Figure S2, A–D). To ask whether the observed changes in myosin activity affected cortical tension, we performed laser-cutting experiments on individual bicellular junctions and measured their initial recoil velocity. Because of the inherent heterogeneity of cell junctional lengths and apical areas across the wing imaginal epithelium, we restricted all laser cuts to the ventral-anterior region of the presumptive wing blade, which normally contains cells with larger apical areas and longer junctions. Additionally, we were careful to avoid proximity to mitotic cells (Supplemental Figure S2E). Consistent with the observed differences in pMRLC staining, we saw a significant decrease in recoil velocities under hypertonic conditions and an even more significant increase in recoil upon hypotonic shift (Figure 2, E and F; Supplemental Movie S1). We observed no correlation between junctional length and recoil velocities (Supplemental Figure S2F). Collectively, these results show that osmotic manipulations can be used to acutely modulate myosin activity and cortical tension in the imaginal epithelium.

To further validate that osmotically altered cortical tension can induce biologically relevant consequences, we once again examined the localization of Yki-YFP. Because tension is known to promote nuclear Yki accumulation, we hypothesized that hypertonic conditions (lower tension) should lead to less nuclear Yki, while hypotonic conditions should result in more nuclear Yki. For these experiments, in order to see a definitive effect on Yki localization, we increased the incubation time to 30 min. Consistent with our hypothesis, shifting tissues from an isotonic to a hypertonic solution resulted in a decrease in nuclear Yki (Supplemental Figure S3, A–B'' and D). Conversely, shifting to a hypotonic solution led to a dramatic increase in nuclear Yki (Supplemental Figure S3, C and D). To further demonstrate the significance of this effect, we decided to first concentrate Yki in the nuclei under hypotonic conditions and then shift to a hypertonic environment. Hypotonically induced nuclear Yki accumulation was completely reversed after incubation in a hypertonic

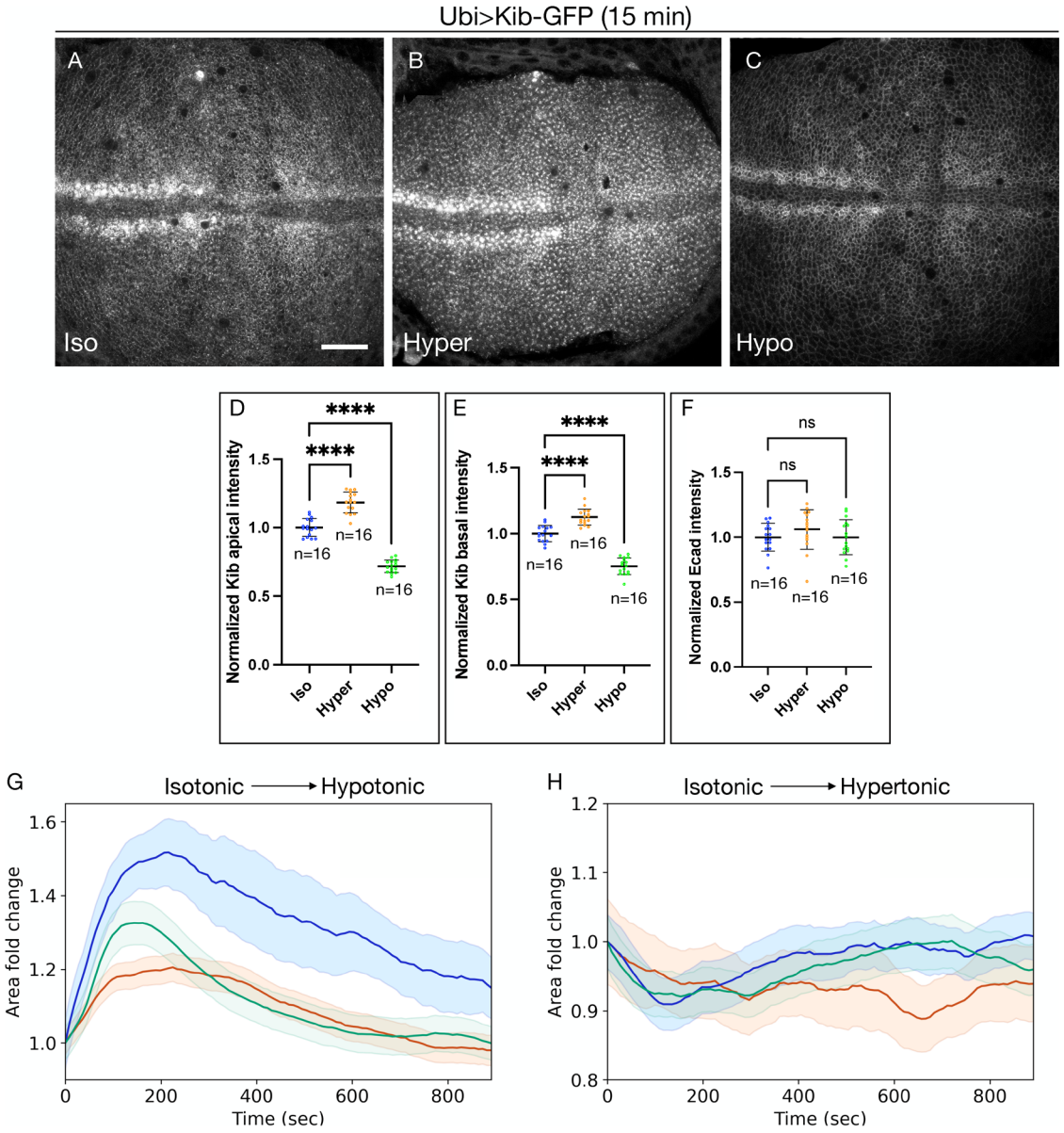

FIGURE 3: Osmotic shifts affect Kib abundance. (A–C) Compared to isotonic conditions (A), hypertonic shift results in higher Kib abundance (B), while hypotonic shift leads to decreased Kib abundance (C). Scale bar = 20 μm. (D–F) Quantification of apical Kib-GFP (D), basal Kib-GFP (E), and apical Ecad-mKate2 (F) mean fluorescence. (G and H) Plots of cell area changes (mean ± SEM) obtained from tissues shifted from isotonic to hypotonic (G) or isotonic to hypertonic (H) conditions. Each curve represents an independent trial/tissue, with three tissues imaged for each condition.

solution (Supplemental Figure S3, E–H). Together, these results show that osmotic manipulations can be used to acutely modulate myosin activity and cortical tension in an epithelial monolayer with biologically relevant consequences.

Osmotic shifts affect Kib abundance

Given our result that changes in the medium osmolarity can influence cortical tension, we asked whether the osmotic manipulations also affected Kib abundance. Compared to isotonic conditions, incubating tissues in a hypertonic solution resulted in an increased Kib abundance at the apical cortex (Figure 3, A, B, and D). Moreover, Kib fluorescence also increased in more basal tissue sections, suggesting that the apical increase in Kib was not due to apical recruitment from the cytoplasmic pool (Figure 3E). Conversely, in tissues incubated in a hypotonic solution, Kib abundance decreased dramatically both at the apical cortex and in more basal tissue sections compared with isotonic controls (Figure 3, C–E). In contrast, fluorescence intensity of Ubi>Kib$^{\Delta WW1}$-GFP did not change significantly under osmotic shifts (Supplemental Figure S4, A–C), suggesting that osmotically-induced Kib degradation is mediated via the previously described Hippo complex-dependent mechanism (Tokamov *et al.*, 2021). These results demonstrate that cortical tension can rapidly modulate Kib abundance.

We also considered the possibility that changes in apical area could alter Kib distribution and fluorescence intensity by concentrating or diluting the protein at the cortex. To address this point, we first measured fluorescence intensity of a junctional marker, Ecad-mKate2, and saw no significant changes under osmotic

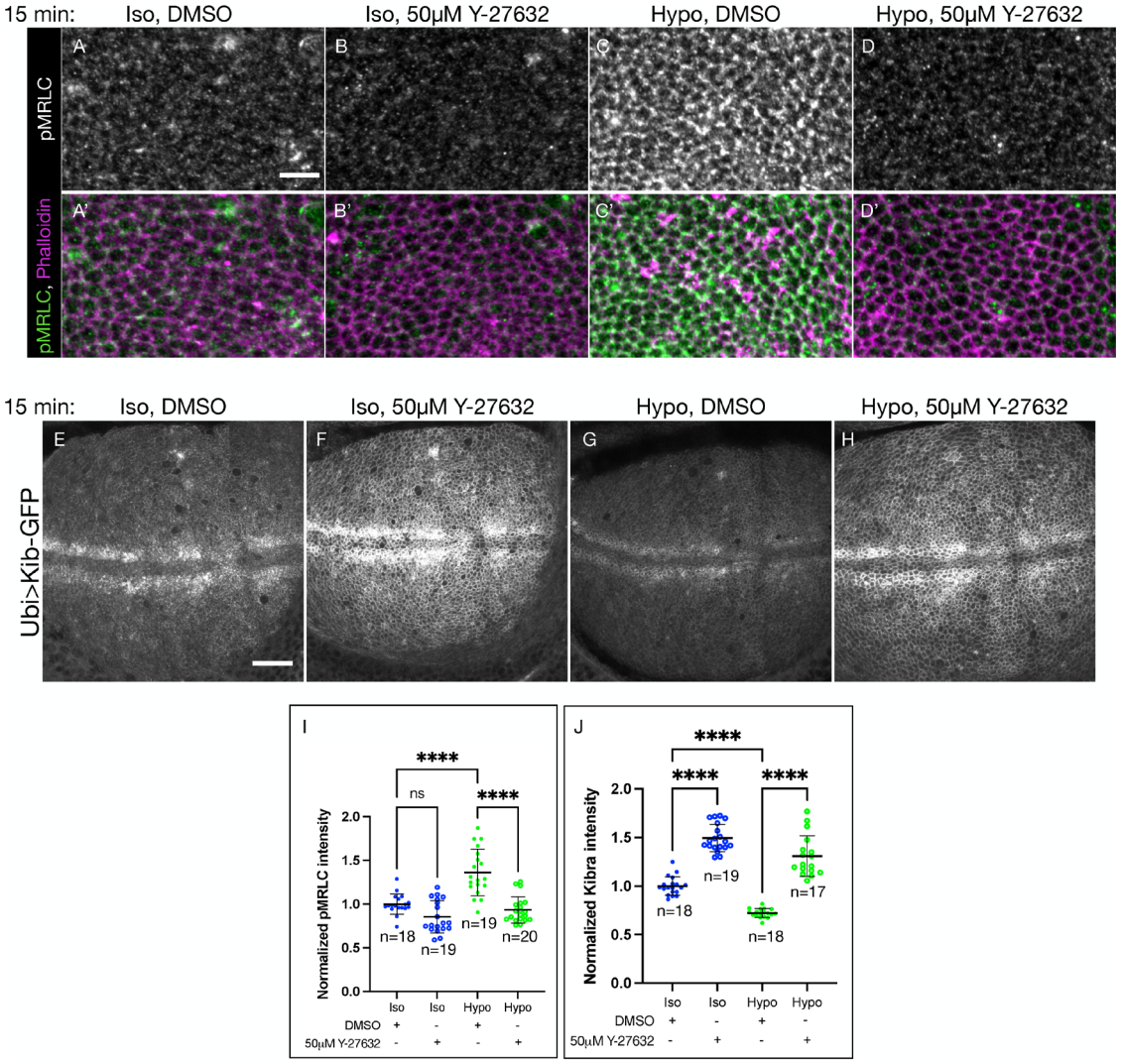

FIGURE 4: Treatment with Y-27632 raises Kib abundance and reverses the effect of hypotonic shift. (A–D′) Staining with the antibody against pMRLC shows that Y-27632 treatment leads to a slight decrease in pMRLC staining under isotonic conditions (A–B′) and a blocks pMRLC upregulation under hypotonic shift (C–D′). Scale bar = 5 μm. (E–H) Compared to control (E), treatment with Y-27632 dramatically increases Kib abundance under isotonic conditions (F). Addition of Y-27632 also blocks the decrease in Kib abundance induced by hypotonic shift (G and H). Scale bar = 20 μm. (I) Plot of normalized mean pMRLC intensities obtained from experiments represented in A–D′. (J) Plot of normalized mean Kib-GFP intensities obtained from experiments represented in E–H.

shifts (Figure 3F). Next, we measured apical cell areas upon shifting wing imaginal tissues from isotonic to hypotonic or hypertonic conditions. Immediately after the addition of the hypotonic solution, apical areas increased rapidly during the first ~3 min of incubation (Figure 3G). However, this initial increase was followed by a steady decrease of areas in the next 12 min, until on average the areas returned roughly to their initial values (Figure 3G; Supplemental Movie S2). Similarly, addition of the hypertonic solution resulted in a transient reduction in apical areas during the first ~3 min, followed by a steady return to their starting values by 15 min of incubation (Figure 3H; Supplemental Movie S3). Because we measured Kib fluorescence after 15 min of incubation (Figure 3, A–C), changes in apical area are unlikely to explain the observed changes in cortical Kib abundance under osmotic shifts. Collectively, these results suggest that changes in myosin activity may be responsible for changes in Kib abundance under osmotic shifts.

Inhibition of myosin activity blocks Kib degradation under hypotonic conditions

If myosin-generated cortical tension is responsible for the observed decrease in Kib abundance under hypotonic shift, then inhibiting myosin activity under these conditions should block Kib degradation. To test this idea, we used Y-27632, a pharmacological inhibitor of Rok activity (Uehata *et al.*, 1997). Under isotonic conditions, we observed a slight reduction in pMRLC staining when tissues were treated with Y-27632 (Figure 4, A–B′), though this effect was not statistically significant (Figure 4I; again, possibly obscured by high antibody background staining). However, Y-27632 potently inhibited myosin hyperactivation induced by hypotonic conditions (Figure 4, C–D′ and I).

We next asked whether Y-27632 treatment would affect Kib abundance. Strikingly, we observed a substantial increase in Kib abundance after 15 min of Y-27632 treatment under isotonic conditions (Figure 4, E, F, and J); supporting the idea that myosin activity

promotes Kib degradation. To test whether Rok inhibition could block the effect of hypotonic conditions, we incubated tissues in a hypotonic solution containing Y-27632. Addition of Y-27632 strongly blocked the effect of the hypotonic medium on Kib abundance (Figure 4, G, H, and J), suggesting that the effect of osmotic shifts on Kib abundance is caused by myosin activity.

We also considered the possibility that the effect of Y-27632 could be mediated via inhibition of another known target of this inhibitor, the atypical protein kinase C (aPKC). To test this possibility, we took advantage of a conditional allele of aPKC, *aPKC^{as4}* that can be acutely inhibited using 1NA-PP1, an allele-specific analog of a potent kinase inhibitor (Hannaford *et al.*, 2019). As expected, under normal conditions, aPKC^{as4} was enriched at the apical cortex in the wing imaginal epithelium (Supplemental Figure S5, A and A'). In contrast, treatment with 1NA-PP1 severely inhibited aPKC cortical localization (Supplemental Figure S5, B and B'). On the other hand, treatment with Y-27632 did not significantly affect aPKC cortical localization in wild-type imaginal discs (Supplemental Figure S5, C–D'). Additionally, we treated wing disks homozygous for *aPKC^{as4}* allele with 1NA-PP1 and did not observe any changes in Kib abundance upon aPKC inhibition (Supplemental Figure S5, E–G). These results show that the effect of Y-27632 on Kib abundance is not due to aPKC inhibition and instead suggest that Kib degradation under hypotonic conditions is mediated via cortical tension.

Par-1 regulates Kib abundance

How can tension influence abundance of a signaling protein such as Kib? Previous work identified a mechanism whereby tension inhibits Hippo signaling via Jub-mediated sequestration and inactivation of Wts/LATS at the cell–cell junctions (Rauskolb *et al.*, 2014; Ibar *et al.*, 2018). Surprisingly, although we observed a significant increase in myosin activity under hypotonic conditions (Figure 2C), we did not detect significant changes in cortical Jub (Supplemental Figure S6, A–D). Additionally, loss of Jub does not affect Kib levels (Supplemental Figure S6E). These observations suggest that cortical tension regulates Kib abundance independently of Jub.

Recently, cortical tension was shown to promote cortical localization of Par-1 in the Drosophila oocyte (Doerflinger *et al.*, 2022). Interestingly, Par-1 mediates proteolytic degradation of a SCF$^{Slimb/\beta TrCP}$ substrate Oskar (Morais-de-Sá *et al.*, 2013) and is known to physically associate with Hippo signaling components and regulate tissue growth (Huang *et al.*, 2013). We therefore hypothesized that cortical tension could promote Kib degradation via Par-1. To test this idea, we first asked whether Par-1 regulates Kib abundance using Ubi>Kib–GFP as a reporter. Kib levels increased significantly upon Par-1 depletion (Figures 5A and C; Supplemental Figure S7A), whereas ectopic Par-1 expression resulted in a significant reduction in Kib levels (Figure 5, B and C). In contrast, loss of Par-1 did not affect the abundance of Kib$^{\Delta WW1}$ (Figure 5, D and E), suggesting that Par-1 regulates Kib levels via Kib-mediated Hippo complex assembly (Tokamov *et al.*, 2021).

Par-1 was previously shown to promote Hpo phosphorylation on Ser30, which inhibits Hpo activity (Huang *et al.*, 2013). Therefore, we considered the possibility that the form of Hpo lacking phosphorylation on Ser30 could be responsible for Kib stabilization under Par-1 depletion. If this were the case, then ectopic expression of Hpo that is refractory to Par-1 phosphorylation (Hpo^{S30A}) would also lead to increased Kib abundance. To this end, we first transiently expressed wild-type Hpo in the posterior compartment of the wing imaginal disc and examined the effect on Kib levels. Consistent with our previous finding that Hpo promotes Kib ubiquitination and degradation (Tokamov *et al.*, 2021), Kib levels decreased significantly under ectopic Hpo expression (Supplemental Figure S7B). Importantly, ectopic expression of Hpo^{S30A} also induced a decrease in Kib abundance (Supplemental Figure S7C), suggesting that the effect of Par-1 on Kib abundance is not mediated through Hpo phosphorylation on Ser30.

We have previously shown that Kib is ubiquitinated via SCF$^{Slimb/\beta TrCP}$ in cultured Schneider's 2 (S2) cells. Because Par-1 is a kinase and is known to function with SCF$^{Slimb/\beta TrCP}$, we asked if Par-1 affects Kib phosphorylation or ubiquitination in S2 cells. To test whether Par-1 promotes Kib phosphorylation, we performed gel-shift assays in the presence of wild type or kinase-dead Par-1 (Par-1^{KD}). Kib is normally phosphorylated in S2 cells, as it appears as a smeary, slow migrating band that collapses into a single, faster migrating band with phosphatase treatment (Figure 5F; Supplemental Figure S7, D and D'; Tokamov *et al.*, 2021). Addition of active Par-1, but not Par-1^{KD}, resulted in disappearance of the lower, non-phosphorylated Kib band, suggesting that Par-1 promotes Kib phosphorylation. Depletion of Par-1 by RNAi did not substantially affect Kib phospho-shift (Figure 5F; Supplemental Figure S7, D and D'), suggesting that Par-1 is not solely responsible for Kib phosphorylation and that not all Par-1-dependent phosphorylation of Kib is detectable in this assay. Regarding the effect of Par-1 on Kib ubiquitination, we observed that while Kib was ubiquitinated in control cells, Par-1 depletion led to a strong decrease in Kib ubiquitination (Figure 5G; Supplemental Figure S7, E and E'). Together, these results suggest that Par-1 regulates ubiquitin-mediated Kib degradation and that tension could modulate Kib abundance via Par-1. However, these data do not distinguish between a structural and a catalytic role for Par-1 in this process.

Cortical tension promotes Par-1 association with the cortex

Given the previous report that myosin activity promotes cortical Par-1 localization in the *Drosophila* oocyte (Doerflinger *et al.*, 2022); we wondered whether a similar effect could be observed in the wing imaginal epithelium. To this end, we first examined Par-1 localization in control cells or in cells overexpressing RhoGEF2. Although known as a basolateral component, in the Drosophila blastoderm Par-1 also localizes at the apicolateral cortex (Bayraktar *et al.*, 2006). In the wing imaginal disc, Par-1 displayed apical and basolateral localization, though its localization appeared diffuse in both places (Figure 6, A and A'). Transient overexpression of RhoGEF2 resulted in sharper Par-1 localization at the cell cortex both apically and basolaterally (Figure 6, B and B'), suggesting that tension can affect Par-1 cortical association. As an alternative approach, we also examined Par-1 localization using Airyscan confocal microscopy under hypotonic conditions. Similar to ectopic RhoGEF2 expression, Par-1 was more tightly associated with the apical and basolateral cortex under hypotonic compared with isotonic conditions (Figure 6, C–D'). These results suggest that tension promotes Par-1 association with the cell cortex.

Par-1 is required for tension-dependent degradation of Kib

We reasoned that if tension regulates in Kib abundance via Par-1, then in the absence of Par-1 tension would have no effect on Kib levels. To test this idea, we depleted Par-1 in the posterior compartment of the wing imaginal disc using the *hh>Gal4* driver and quantified changes in Kib levels when tissues were shifted from isotonic to hypotonic conditions. While we observed a significant decrease in Kib intensity in the anterior (control) compartment, there was no significant change in the posterior (Par-1 depleted) compartment (Figure 6, E–G). Collectively, these results are consistent with the idea that tension modulates Kib abundance by controlling Par-1 cortical association.

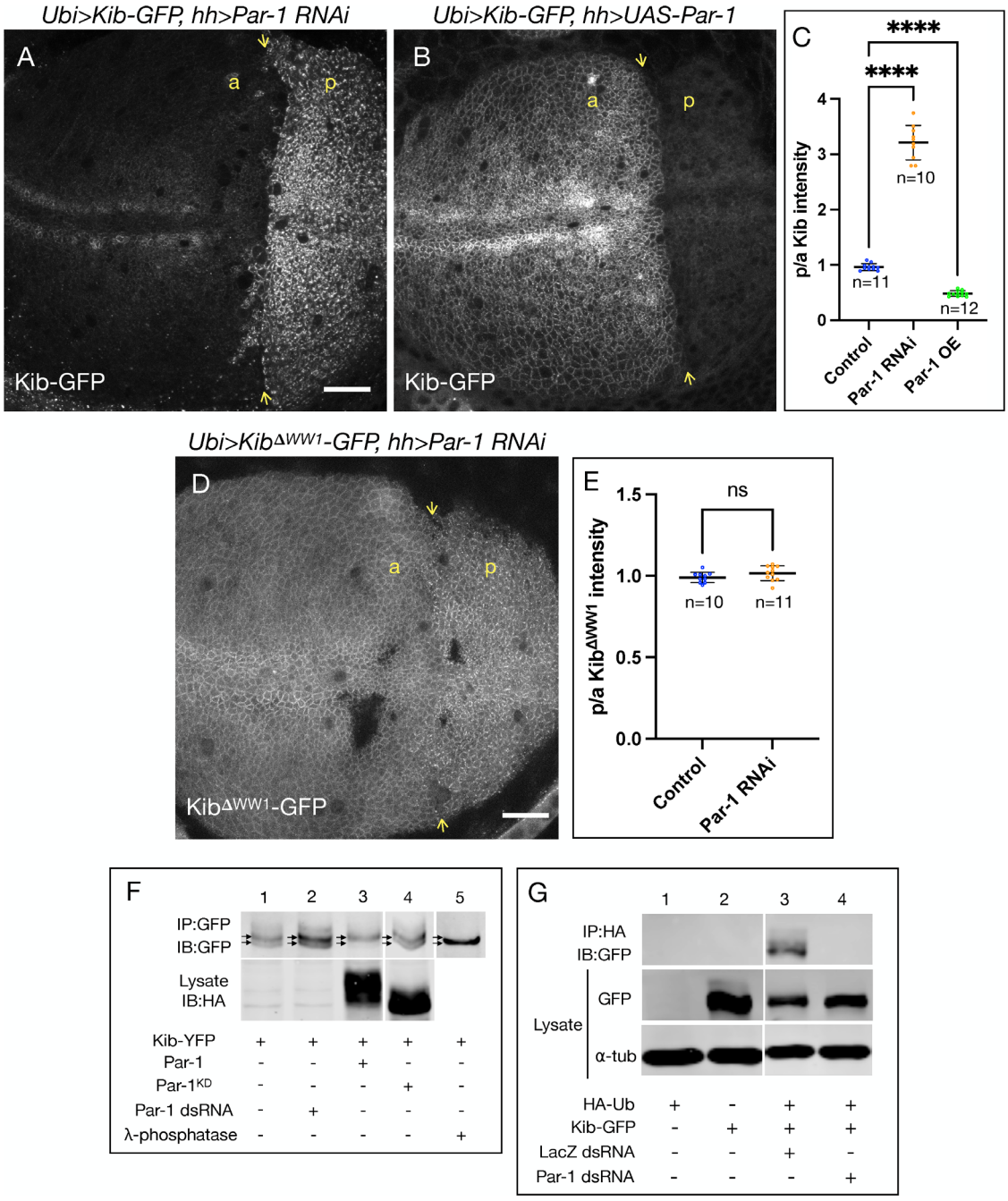

FIGURE 5: Par-1 promotes ubiquitin-mediated Kib degradation. (A) Depletion of Par-1 for 32 hr in the posterior wing disk compartment leads to a dramatic increase in Kib abundance. Yellow arrows indicate the a-p boundary. Scale bar = 20 μm. (B) Ectopic Par-1 expression for 16 hr in the posterior wing disk compartment results in a strong decrease Kib abundance. (C) Quantification of loss or gain of Par-1 functions on Kib abundance as a posterior/anterior (p/a) ratio of mean fluorescence intensity. (D) Loss of Par-1 in the posterior wing disk compartment does not affect $Kib^{\Delta WW1}$ abundance. (E) Quantification of the effect of Par-1 depletion on $Kib^{\Delta WW1}$ abundance as a p/a ratio of mean fluorescence intensity. (F) Kib immunoprecipitated from cultured S2 cells is normally phosphorylated, as evidenced by the slower migrating band (lane 1, upper arrow). Kib treated with λ-phosphatase appears as a single, faster migrating band (lane 5, bottom arrow). Depletion of Par-1 with dsRNA does not have a detectible effect on Kib migration (lane 2). Ectopic expression of wild-type Par-1 but not $Par\text{-}1^{KD}$ leads to decreased abundance of the faster-migrating band (lanes 3 and 4, bottom arrow). (G) Kib immunoprecipitated from cultured S2 cells is normally ubiquitinated when cells are treated with a control LacZ dsRNA (lane 3). Depletion of Par-1 with dsRNA results in decreased Kib ubiquitination (lane 4).

DISCUSSION

Elucidating the molecular mechanisms that control the abundance of individual signaling components has been central to our understanding how the Hippo pathway is regulated (Bosch *et al.*, 2014; Ribeiro *et al.*, 2014; Rodrigues-Campos and Thompson, 2014; Aerne *et al.*, 2015; Ma *et al.*, 2018; Fulford *et al.*, 2019; Misra and Irvine, 2019; Wang *et al.*, 2019; Tokamov *et al.*, 2021). However, how these different mechanisms themselves are regulated, has

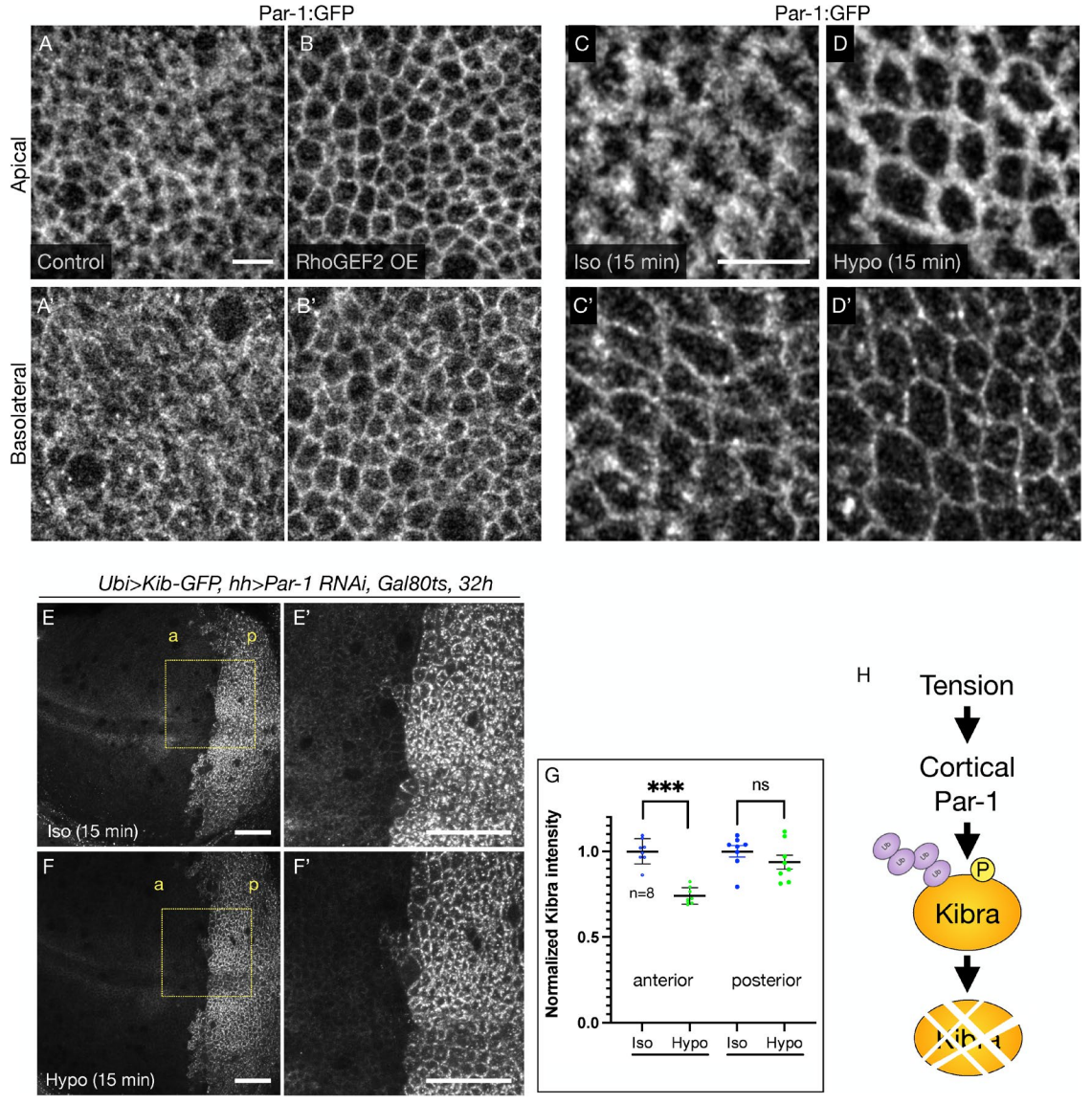

FIGURE 6: Cortical tension regulates Kib abundance by modulating cortical Par-1 association. (A and B′) Compared to control cells (A and A′), ectopic RhoGEF2 expression leads to tighter Par-1 association with the apical and basolateral cell cortex (B and B′). Scale bar = 5 μm. (C and D′) Compared to isotonic conditions (C and C′), Par-1 becomes more tightly associated with the apical and basolateral cell cortex upon hypotonic shift (D and D′). Scale bar = 5 μm. (E–G) Under isotonic conditions, depletion of Par-1 in the posterior compartment (p) leads to a significant increase in Kib levels (E, E′, and G). Shift to hypotonic conditions leads to a significant decrease in Kib abundance in the anterior region, but only a mild (not statistically significant) decrease in the posterior region where Par-1 was depleted (F, F′, and G). Scale bars = 20 μm. (H) A simplified model of Kib degradation by cortical tension and Par-1.

been an intriguing and yet poorly understood area of investigation. Our work reveals a previously unrecognized role of cortical tension in modulating the abundance of a key upstream Hippo pathway component, Kib. Using a combination of genetic, osmotic, and pharmacological approaches, we demonstrate that cortical tension promotes Kib degradation (Figure 6H). Our study also implicates Par-1 in mediating Kib degradation downstream of cortical tension (Figure 6H). This work advances our understanding of how tension regulates Hippo signaling and provides novel insights into the role of mechanical forces in tissue growth and patterning.

We provide several lines of evidence that Kib is degraded as a result of myosin-generated tension. First, we show that activation of myosin via two different myosin light chain kinases, Rok (in the case of ectopic RhoGEF2 expression and Y-27632 treatment) and Strn-MLCK (in the case of ectopic myr–Yki expression) decreases Kib abundance (Figures. 1 and 4), suggesting that Kib degradation occurs irrespective of the upstream mechanisms of myosin activation. Second, although RhoGEF2 is known to promote both myosin activity and formin-mediated F-actin assembly, we did not observe a detectible effect on F-actin under transient RhoGEF2 expression, whereas myosin activity was substantially upregulated (Supplemental Figure S1). Third, we develop a simple, nongenetic and acute approach to dramatically increase myosin activity using hypotonic conditions and demonstrate that myosin activation using this method results in Kib degradation (Figures 2–4). Thus, we propose that Kib degradation is modulated by cortical tension downstream of myosin activity.

Our results also suggest that Kib degradation downstream of cortical tension is mediated via Hippo complex formation. We have shown previously that Kib targets itself for ubiquitin-mediated degradation upon Hippo complex assembly, and this process requires Kib's WW1 domain and a consensus degron motif recognized by $SCF^{Slimb/\beta TrCP}$ (Tokamov *et al.*, 2021). In this study, we observe that the abundance of wild-type Kib, but not $Kib^{\Delta WW1}$, is modulated via myosin activity, raising the question of how tension can promote complex-dependent Kib turnover. In the simplest scenario, cortical tension could promote the association of existing Kib complexes with a tension-sensitive component capable of modulating Kib levels. We identify Par-1 as a potential link in this process. Cortical tension was previously reported to promote cortical Par-1 localization in the *Drosophila* oocyte (Doerflinger *et al.*, 2022). Here, we show that Par-1 promotes turnover of wild-type Kib, but not $Kib^{\Delta WW1}$, in vivo and regulates Kib phosphorylation and ubiquitination in cultured cells (Figure 5). Importantly, cortical tension fails to induce Kib turnover in cells depleted of Par-1 (Figure 6). Based on these results, and our observations that Par-1 becomes more tightly associated with the cell cortex under increased cortical tension (Figure 6), we propose that cortical tension could regulate Kib levels at least in part by modulating the association of Par-1 with Kib signaling complexes. Interestingly, a recent study in human cells also suggested that tension generated at the ECM promotes degradation of an Hpo homologue, MST2, by modulating the physical interaction between MST2 and $SCF^{Slimb/\beta TrCP}$ complex (Fiore *et al.*, 2022). Thus, in a more complex scenario, cortical tension could also regulate Kib association with multiple components of the degradation machinery, including $SCF^{Slimb/\beta TrCP}$.

This study also highlights the recurring role of Par-1 in the regulation of Hippo signaling. Previous work suggested that Par-1 phosphorylates Hpo, which prevents Hpo association with Sav (Huang *et al.*, 2013). Here, we find that Par-1 regulates Kib abundance independently of Hpo phosphorylation. Our observation that Par-1 regulates the abundance of wild-type Kib but not $Kib^{\Delta WW1}$ suggests that Par-1 regulates Kib via the Hippo complex-mediated degradation mechanism involving $SCF^{Slimb/\beta TrCP}$ (Tokamov *et al.*, 2021). This idea is supported by a previous report that Par-1 functions with $SCF^{Slimb/\beta TrCP}$ in promoting turnover of Oscar during Drosophila oocyte development (Morais-de-Sá *et al.*, 2013). Notably, active Par-1 was also found to be a target of $SCF^{Slimb/\beta TrCP}$-mediated degradation (Lee *et al.*, 2012), further highlighting the tight association between Par-1, $SCF^{Slimb/\beta TrCP}$, and Kib. It is still unclear what happens to the rest of the Hippo signaling complex after Kib is degraded, but the multifaceted function of Par-1 in inhibiting Hpo activity, Hpo-Sav interaction, and promoting Kib degradation could provide the means of dissociating the entire signaling complex upon Kib turnover.

One of the surprising observations in our study is that while cortical tension induced by hypotonic conditions triggers Kib degradation, it does not affect junctional Jub accumulation. Previous work has shown that increasing myosin activity via genetic manipulations enhances Jub recruitment to the adherens junctions, where Jub sequesters Wts (Rauskolb *et al.*, 2014). This recruitment is thought to be mediated via tension-induced opening of α-catenin conformation, which exposes a region in α-catenin that binds Jub (Rauskolb *et al.*, 2014; Alégot *et al.*, 2019; Sarpal *et al.*, 2019). Combined with these reports, our observations suggest that hypotonically induced myosin activation may differ from that achieved via common genetic manipulations. Most obviously, this difference could be temporal – hypotonic treatment of wing imaginal discs induces dramatic myosin activation and Kib degradation within 15 min (Figure 2), whereas genetic manipulations are done in the order of hours or days. Thus, α-catenin-mediated recruitment of Jub could occur at a longer timescale compared with the more dynamic Kib turnover. Counter to this argument, a recent study observed rapid junctional accumulation of Jub–Wts clusters at sites of high tension in the Drosophila developing notum (López-Gay *et al.*, 2020). An alternative explanation is that hypotonically induced myosin activation does not result in α-catenin conformational changes. The opening of α-catenin conformation at bicellular junctions is thought to be triggered via actomyosin forces applied orthogonally to the junctions (Rauskolb *et al.*, 2019; López-Gay *et al.*, 2020). This is unlikely to be the case under hypotonic conditions, where actomyosin generated forces would be generated parallel to the lateral membrane to counteract the mechanical stretching induced by hydrostatic pressure.

Finally, our study raises the question of the biological importance of tension-dependent Kib degradation. In the growing wing imaginal epithelium, cortical tension was shown to be higher at the tissue periphery than at the tissue center (LeGoff *et al.*, 2013; Mao *et al.*, 2013). Greater tension at the periphery was proposed to drive growth, possibly via Yki activity, to compensate for the lower concentration of growth-stimulating morphogens, which diffuse from narrow stripes of cells at the center of the tissue (Aegerter-Wilmsen *et al.*, 2007, 2012; Hariharan, 2015; Pan *et al.*, 2016). Additionally, we have previously reported that Kib degradation occurs more prominently at the tissue periphery, where cortical tension is higher (Tokamov *et al.*, 2021). The degree to which tension-mediated Kib degradation affects Yki activity remains a challenging question to test, mainly due to the existence of other tension-sensitive inputs into the pathway (Rauskolb *et al.*, 2014; Deng *et al.*, 2015, 2020; Fletcher *et al.*, 2015; Dutta *et al.*, 2017) and the fact that there are currently no Kib-specific reporters of Hippo pathway activity. Nevertheless, based on previous studies that established Kib as an upstream Hippo signaling regulator (Baumgartner *et al.*, 2010; Genevet *et al.*, 2010; Yu *et al.*, 2010), we propose that tension-mediated Kib degradation could serve to pattern growth via Yki activity across an epithelium such as the wing imaginal disc. Future work is needed to understand how Kib degradation and other tension-regulated mechanisms, such as the Jub–Wts mechanism, are coordinated to control the Hippo pathway and growth. However, this study provides insights for future investigation of the molecular mechanisms by which mechanical forces affect tissue growth.

MATERIALS AND METHODS

Request a protocol through *Bio-protocol*.

Drosophila husbandry

Drosophila melanogaster was cultured using standard techniques at 25°C (unless otherwise noted). For $Gal80^{ts}$ experiments, crosses were maintained at 18°C until larvae reached late second or early third instar stages and shifted to 29°C for the duration specified in each experiment. Immediately after incubation at 29°C, wing imaginal tissues were dissected from wandering third instar larvae and imaged live.

Live imaging

Throughout the study (except in Figures 2, A–C′ and 4, A–D′; Supplemental Figures S1, A–A′ and S5, A–D′), wing imaginal discs were imaged live. Imaging of live tissues was performed as previously described (Xu *et al.*, 2019). Briefly, freshly dissected wing imaginal discs from third instar larvae were pipetted into a ~40 ml droplet of Schneider's Drosophila Medium supplemented with 10% fetal bovine serum (FBS) and mounted on a glass slide. To support the

tissue, spherical glass beads (Cospheric, Product ID: SLGMS-2.5) of ~50 mm in diameter were placed under the coverslip. The mounted samples were immediately imaged.

For osmotic shifts, Y-27632 treatment, and laser ablation experiments, a previously described method for live imaging was used (Restrepo *et al.*, 2016). Briefly, wing imaginal tissues were first dissected in Schneider's Drosophila Medium (Sigma) supplemented with 10% FBS (Thermo Fisher Scientific). The tissues were then transferred with a pipette in 5–10 µl of medium to a glass bottom microwell dish (MatTek, 35-mm petri dish, 14-mm microwell) with No. 1.5 coverglass. The disks were oriented so that the apical side of the disk proper faced the coverglass. A Millicell culture insert (Sigma, 12-mm diameter, 8-µm membrane pore size) was prepared in advance by cutting off the bottom legs with a razor blade and removing any excess membrane material around the rim of the insert. The insert was carefully placed into the 14-mm microwell space, directly on top of the drop containing properly oriented tissues. To prevent the tissue from moving, the space between the insert and the microwell was sealed with ~10 µl of mineral oil. Media with indicated osmolarity and/or chemical inhibitor was then added into the chamber of the insert (200 µl in all experiments). An inverted Zeiss LSM880 laser scanning confocal microscope equipped with a GaAsP spectral detector and the Airyscan module was used for all imaging (except for laser ablation experiments, see below).

Osmotic shift experiments

Schneider's Drosophila Medium (Sigma) supplemented with 10% FBS (Thermo Fisher Scientific) was used as isotonic medium (~360 mOsm). To make a hypertonic solution, the osmolarity of the isotonic solution was increased to ~460 mOsm using 1 M NaCl. To make a hypotonic solution, the isotonic medium was diluted with deionized water to ~216 mOsm. All osmotic solutions were prepared fresh immediately before the experiments. In most experiments, tissues were incubated for 15 min in a humid chamber before mounting (see above). For practical reasons, in laser ablation experiments tissues were incubated for 8 min to allow for measurements to be taken at an average of 15 min under osmotic incubations.

To observe changes in Yki-YFP localization, flies expressing BAC recombineered Yki-YFP in the background of *yki*^{B5} null allele were used. Ubi>RFP^{nls} was also expressed in the background to mark the nuclei. Tissues were dissected and mounted as described above. Each wing disk was first imaged under isotonic conditions, with four to five optical sections taken in the basal plane where the nuclei were clearly identifiable. The isotonic medium was then replaced with an indicated osmotic solution, and after 30 min of incubation, each tissue was reacquired in the same order and roughly the same optical plane. The steps were repeated for the third osmotic condition.

pMRLC staining experiments

Wandering third instar larvae were dissected in an isotonic solution and the wing imaginal discs were transferred into a 150 µl drop of freshly prepared osmotic medium. For experiments with Y-27632, osmotic media with 50 µM of Y-27632 were prepared. The tissues were incubated for 15 min. After incubation, the disks were washed with 1X Ringer's buffer with correspondingly adjusted osmolarity (i.e., for hypertonic experiments, a hypertonic wash was prepared the same way as described above, except 1X Ringer's was used instead of the Schneider's medium) and fixed for 20 min in 2% paraformaldehyde/1X Ringer's solution also with properly adjusted osmolarity (for Y-27632 experiments, 50 µM of Y-27632 was also added in the wash and the fix solutions). Tissues were then stained with the primary antibody against the *Drosophila* phospho-MRLC (anti-pSqh, see Table 1) and secondary antibodies as previously described (McCartney and Fehon, 1996).

Laser ablation of bicellular junctions

Laser cuts were conducted using a pulsed Micropoint nitrogen laser (Andor Technology) tuned to 365 nm and mounted on an Andor Revolution XD spinning disk confocal microscope. Individual junctions were ablated by delivering three pulses at a single point with a duration of 67 ms/pulse. Each tissue was imaged 2× before and 20× immediately after ablation, with a time interval of 4 s. Images were acquired using a 100× oil-immersion lens (Olympus, NA 1.40), an iXon Ultra 897 camera (Andor), and Metamorph (Molecular Devices) as the image acquisition software. Sixteen-bit Z-stacks were collected at each time point consisting of seven slices with 0.5-µm interval.

To measure initial recoil velocity, the positions of the two tricellular vertices connected by the ablated junction were manually tracked using the SIESTA image analysis platform (Fernandez-Gonzalez and Zallen, 2011), and the initial retraction velocities were calculated using custom MATLAB scripts.

Image analysis, quantification of fluorescence intensities, and apical areas

All images were processed in ImageJ. For apical Kib-GFP, Kib$^{\Delta WW1}$-GFP, Jub-GFP, and Ecad-mKate2 mean fluorescence intensity measurements were taken from maximum intensity projections (~0.75 µm/section, four to six sections from apical surface). For basal Kib-GFP mean fluorescence intensity measurements, single basal optical sections were used (~7.5–10 µm below the apical surface). To quantify changes in pMRLC intensity, mean fluorescence measurements were obtained from single most apical sections. Plots and statistical analyses of mean fluorescence intensities were generated using GraphPad Prism software.

To measure changes in apical cell areas under osmotic shifts, cells from Ecad-GFP labeled epithelia were segmented using the Cellpose v1 pretrained "cytoplasm" model (Stringer *et al.*, 2021) and tracked via a previously described tracking algorithm (Williams *et al.*, 2022). Errors in segmentation and tracking were corrected manually. Only cells that remained in the field of view for the entire time-lapse duration were used for quantification. The mean and standard error in cell areas were measured per epithelium. Fold-change in area relative to the start of osmotic shift was plotted using the Matplotlib library in Python.

To quantify nuclear/cytoplasmic Yki–YFP, single optical sections were used. Ubi>RFP channel was used to segment the nuclei using Cellpose and a standard Scikit watershed algorithm (van der Walt *et al.*, 2014) to generate a nuclear mask. The nuclear mask was then applied to Yki–YFP images to extract nuclear Yki–YFP intensities, and the signal outside the nuclear mask was treated as cytoplasmic. The ratios of nuclear to cytoplasmic intensity were then calculated and plotted.

Detection of Kib ubiquitination in S2 cells

Kib ubiquitination assay was performed as described previously (Tokamov *et al.*, 2021). Briefly, ~3.5×10^6 S2 cells (S2-DGRC) were transfected with a total of 500 ng of indicated DNA using dimethyldioctadecylammonium bromide (Sigma; Han, 1996) at 250 mg/ml in six-well plates. pMT-Kib-GFP was cotransfected with pMT-HA-Ub (Zhang *et al.*, 2006) where indicated to provide labeled ubiquitin. To induce expression of the pMT constructs, 700 mM CuSO4 was added to the wells 24 h before cell lysis (2 d after transfection). To

Reagent type (species) or resource	Designation	Source or reference	Identifiers	Additional information
genetic reagent (*D. melanogaster*)	*Ubi>Kib-GFP-FLAG*	(Tokamov *et al.*, 2021)		
genetic reagent (*D. melanogaster*)	*Ubi-Kib$^{\Delta WW1}$-GFP-FLAG*	(Tokamov *et al.*, 2021)		
genetic reagent (*D. melanogaster*)	*UASp-T7-RhoGEF2*	Bloomington Drosophila Stock Center	BL9387	
genetic reagent (*D. melanogaster*)	*UASt-myr-Yki*	10.1016/j.devcel.2018.06.017		
genetic reagent (*D. melanogaster*)	*UAS-Strn RNAi*	Bloomington Drosophila Stock Center	BL26736	Validated in 10.1016/j.devcel.2018.06.017
genetic reagent (*D. melanogaster*)	*UAS-Par-1 RNAi*	Bloomington Drosophila Stock Center	BL32410	
genetic reagent (*D. melanogaster*)	*UAS-jub RNAi*	Bloomington Drosophila Stock Center	BL30806	Validated in 10.1016/j.cub.2010.02.035
genetic reagent (*D. melanogaster*)	*Ecad-3XmKate2*	(Pinheiro *et al.*, 2017)		
genetic reagent (*D. melanogaster*)	*Par-1:GFP (protein trap)*	Bloomington Drosophila Stock Center	BL64452	
genetic reagent (*D. melanogaster*)	*Jub:GFP*	Bloomington Drosophila Stock Center	BL56806	
genetic reagent (*D. melanogaster*)	*w^{1118}; yki^{B5} {yki-YFP} VK37*	(Xu *et al.*, 2018)		
genetic reagent (*D. melanogaster*)	*aPKC^{as4}*	(Hannaford *et al.*, 2019)		
genetic reagent (*D. melanogaster*)	*UAS-hpo*	Laboratory of Nicholas Tapon, Francis Crick Institute		
genetic reagent (*D. melanogaster*)	*UAS-hpo^{S30A}*	(Huang *et al.*, 2013)		
Antibody	anti-pSqh (Guinea pig, polyclonal)	(Zhang and Ward, 2011)		Tissue staining (1:300)
Antibody	anti-DEcad (Rat, polyclonal)	Developmental Studies Hybridoma Bank	Catalogue#AB_528120; RRID:AB_528120	Tissue staining (1:1000)
Antibody	anti-PKC, rabbit polyclonal	Santa Cruz Biotechnology	Lot#: G2304	Tissue staining (1:1000)
Antibody	anti-GFP, guinea pig, polyclonal	(Yee *et al.*, 2019)		IP (1:1250)
Antibody	anti-GFP, rabbit, polyclonal	Michael Glotzer, (University of Chicago)		IB (1:5000)
Chemical	Y-27632	Fisher Scientific	Catalogue# 12541	Rok inhibitor
Chemical	1-NA-PP1	Cayman	Catalogue# CAYM-10954-1	ATP analogue
Cell line	S2: S2-DRSC, *D. melanogaster*	Laboratory of Peter Cherbas	RRID:CVCL_TZ72	

TABLE 1: *Drosophila* stocks and other reagents used in this study.

inhibit proteasomal degradation, 50 mM MG132 (Cayman Chemical) and 50 mM calpain inhibitor I (Sigma Aldrich) were added 4 h before cell lysis. Cells were lysed in RIPA buffer (150 mM NaCl, 1% NP-40, 0.5% Na deoxycholate, 0.1% sodium dodecyl sulfate, and 25 mM Tris [50 mM, pH 7.4]), supplemented with 5 mM N-ethylmaleimide and Complete protease inhibitor cocktail (Roche, one tablet/10 ml of buffer). HA-tagged ubiquitin was purified using Pierce anti-HA magnetic beads (clone 2–2.2.14). Lysates and IP samples were run on 8% polyacrylamide gel and ubiquitinated Kib in the IP samples was detected by Western Blot using anti-GFP antibody (rabbit, see Table 1).

Detection of Kib phosphorylation in S2 cells

pMT-Kib-GFP and pAHW-Par-1 or pAHW-Par-1^{KD} (gift from Bingwei Lu, Stanford University) were transfected and expression was

induced as described above. Immunoprecipitation (IP) was performed 3 d after transfection. To induce expression of pMT-Kib-GFP, 700 mM CuSO4 was added to the wells 24 h before cell lysis (2 d after transfection).

Cells were harvested and lysed on ice in buffer containing 25 mM HEPES, 150 mM NaCl, 1 mM ethylenediaminetetraacetic acid, 0.5 mM ethylene glycol-bis(b-aminoethyl ether)-N, N, N0, N0-tetraacetic acid, 0.9 M glycerol, 0.1% Triton X-100, 0.5 mM Dithiothreitol, and Complete protease inhibitor (Roche) and PhosSTOP (Sigma Aldrich) phosphatase inhibitor cocktails at one tablet/10 ml concentration each. Cell lysates were then incubated with anti-GFP antibody (guinea pig, see Table 1) for 30 min. Antibody-bound Kib-GFP was pulled down using Pierce Protein A magnetic beads (Thermo Fisher Scientific) for 1.5 h. A control immunoprecipitated sample was treated with λ-phosphatase. Samples were run on 8% polyacrylamide gel, with 118:1 acrylamide/bisacrylamide (Scheid *et al.*, 1999), to better resolve phosphorylated Kib species. Kib was detected by Western Blot using anti-GFP antibody (rabbit, see Table 1).

ACKNOWLEDGMENTS

We thank Bingwei Lu, Lei Zhang, Jin Jiang, Developmental Studies Hybridoma Bank, and the Bloomington stock center for fly stocks and other reagents. We also thank Katheryn Rothenberg for help with laser ablation experiments. S.A.T. was supported by a training grant from the National Institutes of Health (NIH-T32 GM007183) and National Science Foundation-Graduate Research Fellowship Program. A.M.W. was funded by National Institutes of Health T32 HD055164GS and by grants from the National Institutes of Health to S.H.B. (R01 GM126047 and R35 GM148485). G.S. was supported by an Ontario Graduate Scholarship, an Alexander Graham Bell Canada Graduate Scholarship from the Natural Sciences and Engineering Research Council of Canada (NSERC), and grants from the Canadian Institutes of Health Research to R.F.G. (156279 and 186188). This work was supported by a grant from the National Institutes of Health to R.G.F. (R01NS034783).

REFERENCES

Aegerter-Wilmsen T, Aegerter CM, Hafen E, Basler K (2007). Model for the regulation of size in the wing imaginal disc of Drosophila. Mech Dev 124, 318–326.

Aegerter-Wilmsen T, Heimlicher MB, Smith AC, de Reuille PB, Smith RS, Aegerter CM, Basler K (2012). Integrating force-sensing and signaling pathways in a model for the regulation of wing imaginal disc size. Development 139, 3221–3231.

Aerne BL, Gailite I, Sims D, Tapon N (2015). Hippo stabilises its adaptor salvador by antagonising the HECT ubiquitin ligase Herc4. PLOS ONE 10, e0131113.

Alégot H, Markosian C, Rauskolb C, Yang J, Kirichenko E, Wang Y-C, Irvine KD (2019). Recruitment of Jub by α-catenin promotes Yki activity and *Drosophila* wing growth. J Cell Sci 132, jcs222018.

Aragona M, Panciera T, Manfrin A, Giulitti S, Michielin F, Elvassore N, Dupont S, Piccolo S (2013). A mechanical checkpoint controls multicellular growth through YAP/TAZ regulation by actin-processing factors. Cell 154, 1047–1059.

Baumgartner R, Poernbacher I, Buser N, Hafen E, Stocker H (2010). The WW domain protein Kibra acts upstream of Hippo in Drosophila. Dev Cell 18, 309–316.

Bayraktar J, Zygmunt D, Carthew RW (2006). Par-1 kinase establishes cell polarity and functions in Notch signaling in the *Drosophila* embryo. J Cell Sci 119, 711–721.

Bosch JA, Sumabat TM, Hafezi Y, Pellock BJ, Gandhi KD, Hariharan IK (2014). The Drosophila F-box protein Fbxl7 binds to the protocadherin Fat and regulates Dachs localization and Hippo signaling. ELife 3, e03383.

Boulant S, Kural C, Zeeh J-C, Ubelmann F, Kirchhausen T (2011). Actin dynamics counteract membrane tension during clathrin-mediated endocytosis. Nat Cell Biol 13, 1124–1131.

Deng H, Wang W, Yu J, Zheng Y, Qing Y, Pan D (2015). Spectrin regulates Hippo signaling by modulating cortical actomyosin activity. eLife 4, e06567.

Deng H, Yang L, Wen P, Lei H, Blount P, Pan D (2020). Spectrin couples cell shape, cortical tension, and Hippo signaling in retinal epithelial morphogenesis. J Cell Biol 219, e201907018.

Di Ciano C, Nie Z, Szászi K, Lewis A, Uruno T, Zhan X, Rotstein OD, Mak A, Kapus A (2002). Osmotic stress-induced remodeling of the cortical cytoskeleton. Am J Physiol-Cell Physiol 283, C850–C865.

Diz-Muñoz A, Thurley K, Chintamen S, Altschuler SJ, Wu LF, Fletcher DA, Weiner OD (2016). Membrane tension acts through PLD2 and mTORC2 to limit actin network assembly during neutrophil migration. PLOS Biol 14, e1002474.

Doerflinger H, Zimyanin V, St Johnston D (2022). The Drosophila anterior-posterior axis is polarized by asymmetric myosin activation. Curr Biol 32, 374–385.e4.

Dupont S, *et al.* (2011). Role of YAP/TAZ in mechanotransduction. Nature 474, 179–183.

Dutta S, Capelli SM, Paramasivam M, Dasgupta I, Cirka H, Billiar K, McCollum D (2017). TRIP6 inhibits Hippo signaling in response to tension at adherens junctions. EMBO Rep 19, 337–350.

Fernandez BG, Gaspar P, Bras-Pereira C, Jezowska B, Rebelo SR, Janody F (2011). Actin-Capping protein and the Hippo pathway regulate F-actin and tissue growth in Drosophila. Development 138, 2337–2346.

Fernandez-Gonzalez R, Zallen JA (2011). Oscillatory behaviors and hierarchical assembly of contractile structures in intercalating cells. Phys Biol 8, 045005.

Fiore APZP, Rodrigues AM, Ribeiro-Filho HV, Manucci AC, de Freitas Ribeiro P, Botelho MCS, Vogel C, Lopes-de-Oliveira PS, Pagano M, Bruni-Cardoso A (2022). Extracellular matrix stiffness regulates degradation of MST2 via SCF βTrCP. Biochim Biophys Acta BBA - Gen Subj 1866, 130238.

Fletcher GC, Elbediwy A, Khanal I, Ribeiro PS, Tapon N, Thompson BJ (2015). The Spectrin cytoskeleton regulates the Hippo signalling pathway. EMBO J 34, 940–954.

Fulford AD, Holder MV, Frith D, Snijders AP, Tapon N, Ribeiro PS (2019). Casein kinase 1 family proteins promote Slimb-dependent Expanded degradation. ELife 8, e46592.

Genevet A, Wehr MC, Brain R, Thompson BJ, Tapon N (2010). Kibra is a regulator of the Salvador/Warts/Hippo signaling network. Dev Cell 18, 300–308.

Guilak F, Erickson GR, Ting-Beall HP (2002). The effects of osmotic stress on the viscoelastic and physical properties of articular chondrocytes. Biophys J 82, 720–727.

Hamaratoglu F, Willecke M, Kango-Singh M, Nolo R, Hyun E, Tao C, Jafar-Nejad H, Halder G (2006). The tumour-suppressor genes NF2/Merlin and Expanded act through Hippo signalling to regulate cell proliferation and apoptosis. Nat Cell Biol 8, 27–36.

Han K (1996). An efficient DDAB-mediated transfection of Drosophila S2 cells. Nucleic Acids Res 24, 4362–4363.

Hannaford M, Loyer N, Tonelli F, Zoltner M, Januschke J (2019). A chemical-genetics approach to study the role of atypical Protein Kinase C in *Drosophila*. Development 146, dev170589.

Hariharan IK (2015). Organ size control: lessons from Drosophila. Dev Cell 34, 255–265.

Huang H-L, *et al.* (2013). Par-1 Regulates tissue growth by influencing Hippo phosphorylation status and Hippo-Salvador association. PLoS Biol 11, e1001620.

Ibar C, Kirichenko E, Keepers B, Enners E, Fleisch K, Irvine KD (2018). Tension-dependent regulation of mammalian Hippo signaling through LIMD1. J Cell Sci 131, jcs214700.

Lecuit T, Lenne P-F, Munro E (2011). Force generation, transmission, and integration during cell and tissue morphogenesis. Annu Rev Cell Dev Biol 27, 157–184.

Lee S, Wang J-W, Yu W, Lu B (2012). Phospho-dependent ubiquitination and degradation of PAR-1 regulates synaptic morphology and tau-mediated Aβ toxicity in Drosophila. Nat Commun 3, 1312.

LeGoff L, Rouault H, Lecuit T (2013). A global pattern of mechanical stress polarizes cell divisions and cell shape in the growing *Drosophila* wing disc. Development 140, 4051–4059.

López-Gay JM, *et al.* (2020). Apical stress fibers enable a scaling between cell mechanical response and area in epithelial tissue. Science 370, eabb2169.

Ma X, Guo X, Richardson HE, Xu T, Xue L (2018). POSH regulates Hippo signaling through ubiquitin-mediated expanded degradation. Proc Natl Acad Sci 115, 2150–2155.

Mao Y, Tournier AL, Hoppe A, Kester L, Thompson BJ, Tapon N (2013). Differential proliferation rates generate patterns of mechanical tension that orient tissue growth. EMBO J 32, 2790–2803.
McCartney BM, Fehon RG (1996). Distinct cellular and subcellular patterns of expression imply distinct functions for the Drosophila homologues of moesin and the neurofibromatosis 2 tumor suppressor, merlin. J Cell Biol 133, 843–852.
Misra JR, Irvine KD (2019). Early girl is a novel component of the Fat signaling pathway. PLOS Genet 15, e1007955.
Morais-de-Sá E, Vega-Rioja A, Trovisco V, St Johnston D (2013). Oskar is targeted for degradation by the sequential action of Par-1, GSK-3, and the SCF-Slimb ubiquitin ligase. Dev Cell 26, 303–314.
Pan Y, Heemskerk I, Ibar C, Shraiman BI, Irvine KD (2016). Differential growth triggers mechanical feedback that elevates Hippo signaling. Proc Natl Acad Sci 113, E6974–E6983.
Piekny A, Werner M, Glotzer M (2005). Cytokinesis: welcome to the Rho zone. Trends Cell Biol 15, 651–658.
Pietuch A, Brückner BR, Janshoff A (2013). Membrane tension homeostasis of epithelial cells through surface area regulation in response to osmotic stress. Biochim Biophys Acta BBA - Mol Cell Res 1833, 712–722.
Pinheiro D, *et al*. (2017). Transmission of cytokinesis forces via E-cadherin dilution and actomyosin flows. Nature 545, 103–107.
Rauskolb C, Cervantes E, Madere F, Irvine KD (2019). Organization and function of tension-dependent complexes at adherens junctions. J Cell Sci 132, jcs224063.
Rauskolb C, Sun S, Sun G, Pan Y, Irvine KD (2014). Cytoskeletal tension inhibits Hippo signaling through an Ajuba-Warts complex. Cell 158, 143–156.
Restrepo S, Zartman JJ, Basler K (2016). Cultivation and live imaging of Drosophila imaginal discs. Methods Mol Biol Clifton NJ 1478, 203–213.
Ribeiro P, Holder M, Frith D, Snijders AP, Tapon N (2014). Crumbs promotes expanded recognition and degradation by the SCFSlimb/-TrCP ubiquitin ligase. Proc Natl Acad Sci 111, E1980–E1989.
Rodrigues-Campos M, Thompson BJ (2014). The ubiquitin ligase FbxL7 regulates the Dachsous-Fat-Dachs system in Drosophila. Development 141, 4098–4103.
Roffay C, *et al*. (2021). Passive coupling of membrane tension and cell volume during active response of cells to osmosis. Proc Natl Acad Sci 118, e2103228118.
Sansores-Garcia L, Bossuyt W, Wada K-I, Yonemura S, Tao C, Sasaki H, Halder G (2011). Modulating F-actin organization induces organ growth by affecting the Hippo pathway. EMBO J 30, 2325–2335.
Sarpal R, Yan V, Kazakova L, Sheppard L, Yu JC, Fernandez-Gonzalez R, Tepass U (2019). Role of α-Catenin and its mechanosensing properties in regulating Hippo/YAP-dependent tissue growth. PLOS Genet 15, e1008454.
Scheid MP, Schubert KM, Duronio V (1999). Regulation of Bad phosphorylation and association with Bcl-xL by the MAPK/Erk kinase*. J Biol Chem 274, 31108–31113.
Sinha B, *et al*. (2011). Cells respond to mechanical stress by rapid disassembly of caveolae. Cell 144, 402–413.
Stewart MP, Helenius J, Toyoda Y, Ramanathan SP, Muller DJ, Hyman AA (2011). Hydrostatic pressure and the actomyosin cortex drive mitotic cell rounding. Nature 469, 226–230.
Stringer C, Wang T, Michaelos M, Pachitariu M (2021). Cellpose: a generalist algorithm for cellular segmentation. Nat Methods 18, 100–106.
Su T, Ludwig MZ, Xu J, Fehon RG (2017). Kibra and Merlin activate the Hippo pathway spatially distinct from and independent of expanded. Dev Cell 40, 478–490.e3.
Tokamov SA, Nouri N, Rich A, Buiter S, Glotzer M, Fehon RG (2023). Apical polarity and actomyosin dynamics control Kibra subcellular localization and function in Drosophila Hippo signaling. Dev Cell 58, 1864–1879.e4.
Tokamov SA, Su T, Ullyot A, Fehon RG (2021). Negative feedback couples Hippo pathway activation with Kibra degradation independent of Yorkie-mediated transcription. ELife 10, e62326.
Uehata M, *et al*. (1997). Calcium sensitization of smooth muscle mediated by a Rho-associated protein kinase in hypertension. Nature 389, 990–994.
Wada K-I, Itoga K, Okano T, Yonemura S, Sasaki H (2011). Hippo pathway regulation by cell morphology and stress fibers. Development 138, 3907–3914.
van der Walt S, Schönberger JL, Nunez-Iglesias J, Boulogne F, Warner JD, Yager N, Gouillart E, Yu T (2014). scikit-image: image processing in Python. PeerJ 2, e453.
Wang X, Zhang Y, Blair SS (2019). Fat-regulated adaptor protein Dlish binds the growth suppressor Expanded and controls its stability and ubiquitination. Proc Natl Acad Sci 116, 1319–1324.
Williams AM, Donoughe S, Munro E, Horne-Badovinac S (2022). Fat2 polarizes the WAVE complex in trans to align cell protrusions for collective migration. ELife 11, e78343.
Xu J, Su T, Tokamov SA, Fehon RG (2019). Live imaging of Hippo pathway components in Drosophila imaginal discs. In: The Hippo Pathway, ed. A Hergovich, New York, NY: Springer New York, 53–59.
Xu J, Vanderzalm PJ, Ludwig M, Su T, Tokamov SA, Fehon RG (2018). Yorkie functions at the cell cortex to promote Myosin activation in a non-transcriptional manner. Dev Cell 46, 271–284.e5.
Yee WB, Delaney PM, Vanderzalm PJ, Ramachandran S, Fehon RG (2019). The CAF-1 complex couples Hippo pathway target gene expression and DNA replication. Mol Biol Cell 30, 2929–2942.
Yu J, Zheng Y, Dong J, Klusza S, Deng W-M, Pan D (2010). Kibra functions as a tumor suppressor protein that regulates Hippo signaling in conjunction with Merlin and expanded. Dev Cell 18, 288–299.
Zhang L, Ward RE (2011). Distinct tissue distributions and subcellular localizations of differently phosphorylated forms of the myosin regulatory light chain in Drosophila. Gene Expr Patterns 11, 93–104.
Zhang Q, Zhang L, Wang B, Ou C-Y, Chien C-T, Jiang J (2006). A Hedgehog-induced BTB protein modulates Hedgehog signaling by degrading Ci/Gli transcription factor. Dev Cell 10, 719–729.